RSC Applied Polymers

ROYAL SOCIETY OF CHEMISTRY

PAPER

View Article Online
View Journal

Cite this: DOI: 10.1039/d5lp00379b

Multi-responsive polymers with degradable side-chain functionality for controlled hydrolysis and tunable thermal transition

Maryam Behzad Khoshgoee,†[a] Mithun Kumar Debnath,†[a] Griffin Pardo,[a] Yichun Yuan,[a] Muhammad Zeeshan,[b,c] Erqian Mao,[a] Thomas G. Gray,[a] Burcu Gurkan,[b] Matthew J. Bertin[a] and Metin Karayilan*[a]

Stimuli-responsive polymers that integrate environmental sensitivity with controlled degradation offer powerful opportunities for next-generation biomedical materials. Here, we introduce a new class of multi-responsive terpolymers synthesized *via* reversible addition–fragmentation chain-transfer (RAFT) polymerization, incorporating comonomers with hydrolytically labile lactone (LMA) or cyclic carbonate (C^2MA) side chains into thermoresponsive oligo(ethylene glycol)-based systems. By systematically tuning monomer composition, we achieved controlled modulation of cloud point temperature (T_{cp}), viscosity, and degradation kinetics within the physiologically relevant window (25–37 °C). Cyclic carbonate-containing terpolymers exhibited lower viscosity, lower glass transition temperatures, and faster hydrolysis than lactone analogues, enabling facile injectability and time-dependent solubility transitions. Density functional theory (DFT) calculations revealed distinct transition state geometries and energetics for lactone *versus* carbonate ring-opening, with cyclic carbonate hydrolysis kinetically favored. Hydrolysis-driven shifts in T_{cp} linked side-chain chemistry to temporal control of thermal phase behavior. Notably, radiofrequency (RF)-induced heating triggered a rapid, localized temperature increase for lactone and cyclic carbonate terpolymers, demonstrating the potential for remote, on-demand actuation. Injectability tests in tissue-mimicking matrices revealed qualitatively sustained, localized release profiles governed by polymer viscosity and degradation rates. Consistent with these observations, dialysis-based dye release studies demonstrated composition-dependent release kinetics, where cyclic carbonate terpolymers exhibited faster payload release relative to lactone analogues. Collectively, this work establishes a versatile platform of hydrolytically and thermally programmable polymers, uniquely integrating physiological responsiveness with potential external triggering mechanisms for applications in injectable therapeutics, tissue adhesives, and smart biomedical interfaces.

Received 26th November 2025,
Accepted 25th March 2026

DOI: 10.1039/d5lp00379b

rsc.li/rscapplpolym

1. Introduction

Stimuli-responsive polymers[1–6] capable of undergoing structural or solubility transitions in response to environmental or external triggers such as temperature,[7,8] pH,[9,10] light,[11] glucose,[12,13] or enzymatic activity[14] have emerged as useful tools for next-generation biomedical materials. Among these, thermoresponsive polymers, those that exhibit a reversible phase transition at the lower critical solution temperature (LCST), are particularly attractive for biomedical applications, as they can be engineered to respond near physiological temperatures with reversible phase behavior, enabling injectable systems, controlled release platforms, and smart scaffolds for tissue engineering.[15–18] Thermoresponsive injectable polymers are especially valuable due to their ability to transition *in situ* from a liquid to a gel state, conform to irregular anatomical geometries, and provide minimally invasive medical interventions, including drug delivery, bioimaging, regenerative medicine, and tissue adhesives.[19–21]

These thermoresponsive materials typically exhibit coil-to-globule transitions in aqueous environments, becoming insoluble as temperature exceeds the LCST, driven by the disruption of polymer-water hydrogen bonding and the dominance of intrachain hydrophobic interactions. Classical LCST-type materials include poly(*N*-isopropylacrylamide) (PNIPAM),[22,23] poly(oligo(ethylene glycol) methacrylate) (POEGMA),[24,25] and

[a]*Department of Chemistry, Case Western Reserve University, Cleveland, Ohio 44106, USA. E-mail: metin.karayilan@case.edu*
[b]*Department of Chemical and Biomolecular Engineering, Case Western Reserve University, Cleveland, Ohio 44106, USA*
[c]*Department of Mechanical Engineering, Massachusetts Institute of Technology, Cambridge, MA 02139, USA*
†These authors contributed equally.

poly(2-oxazoline)[26,27] derivatives, which exhibit sharp, tunable transitions. The thermal response of these polymers can be tailored by modulating polymer architecture, copolymer composition, end-group functionalization, and hydrophilic–hydrophobic balance.[7] For instance, copolymerization of oligo(ethylene glycol) methacrylate derivatives with varying side–chain lengths allows systematic adjustment of LCST over a wide range of temperatures while maintaining biocompatibility and minimal hysteresis.[28] To enhance their functional scope, recent strategies have focused on introducing hydrolyzable side chains such as lactones[29] and cyclic acetals.[30,31] These degradable groups impart time-dependent solubility and LCST shifts by gradually increasing polymer hydrophilicity as hydrolysis proceeds.

For instance, Vernon *et al.* reported that copolymers of NIPAM with dimethyl-γ-butyrolactone acrylate (DBA), undergoing *in situ* gelation, have demonstrated hydrolysis-triggered elevation in LCST due to ring-opening of the lactone moieties, which increases hydrophilicity and promotes gradual resorption and dissolution *in vivo*.[29] These polymers have been shown to undergo self-catalytic hydrolysis, making them ideal for injectable, *in situ*-forming systems. This property has been particularly beneficial in designing injectable delivery systems with temporal control over material dissolution and payload release. Similarly, *in vivo* studies of PNIPAM-based copolymers containing DBA and acrylic acid demonstrated that the inclusion of acidic comonomers accelerated hydrolysis, leading to a gradual increase in LCST.[32–35] However, these PNIPAM-based copolymers are often limited by the relatively low incorporation of degradable lactone comonomers, which constrains the extent and tunability of the hydrolysis response. The resulting LCST shifts can fall outside the physiologically relevant window at higher lactone monomer incorporation, potentially compromising injectability, sol–gel behavior, and application performance *in vivo*.

Beyond lactones, dioxolane (cyclic acetal)-functionalized monomers provide an alternative strategy for introducing hydrolytic sensitivity. For example, Kizhakkedathu and coworkers synthesized poly(*N*-acrylamide) with dioxolane side chains, which underwent partial hydrolysis of pendant dioxolane groups to generate diol functionalities, resulting in tunable LCST behavior.[30] Acetal- and ketal-functional polymers further extend this concept by enabling acid-catalyzed hydrolysis in mildly acidic environments, such as tumor microenvironments or intracellular compartments. Recently, poly(2-oxazoline)-based systems bearing pH-cleavable acetal side chains have been developed by Hoogenboom *et al.* to achieve dual responsiveness, wherein mild acid exposure triggers hydrolysis, increases hydrophilicity, and disrupts micelle structures to release payloads.[31] These systems show strong stability at pH 7.4 but undergo rapid transformation and solubilization at pH 4–5, illustrating the value of degradable side chains in tuning polymer behavior and function. However, the concurrent release of aldehyde- or ketone-containing small molecule byproducts during hydrolysis of cyclic acetal-based degradable groups[36,37] should also be considered, as these species may contribute to local cytotoxicity or impose metabolic burden in sensitive biomedical environments.

Complementing internal cues, unconventional externally triggered stimuli-responsive polymers offer remote, spatiotemporal control over structural or chemical transformations in response to applied physical triggers such as ultrasound,[38–41] microwave radiation,[42] or magnetic fields.[43] These smart systems offer a unique opportunity for remote, controlled activation of molecular release, structural changes, or functional responses, making them particularly attractive for targeted drug delivery, tissue engineering, bioimaging, and shape memory polymer applications.[44–46] However, their translational potential is often limited by the need for highly specialized, biocompatible triggering devices and energy sources that must operate safely and effectively under physiological conditions. This constraint underlines the importance of designing polymer systems that are both sensitive to mild, clinically relevant stimuli and robust under biological constraints.

These advancements highlight the value of integrating degradable functional groups with thermoresponsive backbones to create dual-responsive polymers capable of time-dependent and environment-triggered transitions. Such systems enable highly programmable control over solubility, gelation, degradation, and release, with promising implications for injectable therapeutics, on-demand drug delivery, and smart biomaterial interfaces. Herein, we report the design, synthesis, and characterization of a new class of dual-responsive PEG-based thermoresponsive terpolymers incorporating hydrolyzable γ-butyrolactone or cyclic glycerol carbonate side chains (Fig. 1). To our knowledge, this work represents the first incorporation of lactone functionality into PEG-based thermoresponsive systems and the first demonstration of cyclic carbonate units in stimuli-responsive polymer platforms. Lactone and cyclic carbonate[47,48] functional groups were selected for their ability to undergo hydrolytic degradation under physiologically relevant conditions, enabling time-dependent increases in polymer hydrophilicity and tunable LCST behavior, critical features for injectable and resorbable biomaterials. These characteristics make them particularly advantageous for drug delivery systems that require predictable degradation and sustained performance. By directly comparing these two functional groups, this study aims to elucidate how their distinct hydrolysis kinetics and degradation pathways impact key material properties, including injectability, thermal transitions, responsiveness to external radiofrequency (RF) stimulation, and dye release behavior.

2. Materials and methods

2.1. Materials

Oligo(ethylene glycol) methyl ether methacrylate (OEGMA, M_n = 500 g mol^{-1}, Sigma-Aldrich) and di(ethylene glycol) methyl ether methacrylate (DEGMA, 95%, Sigma-Aldrich) were passed through a neutral alumina column to remove inhibitors.

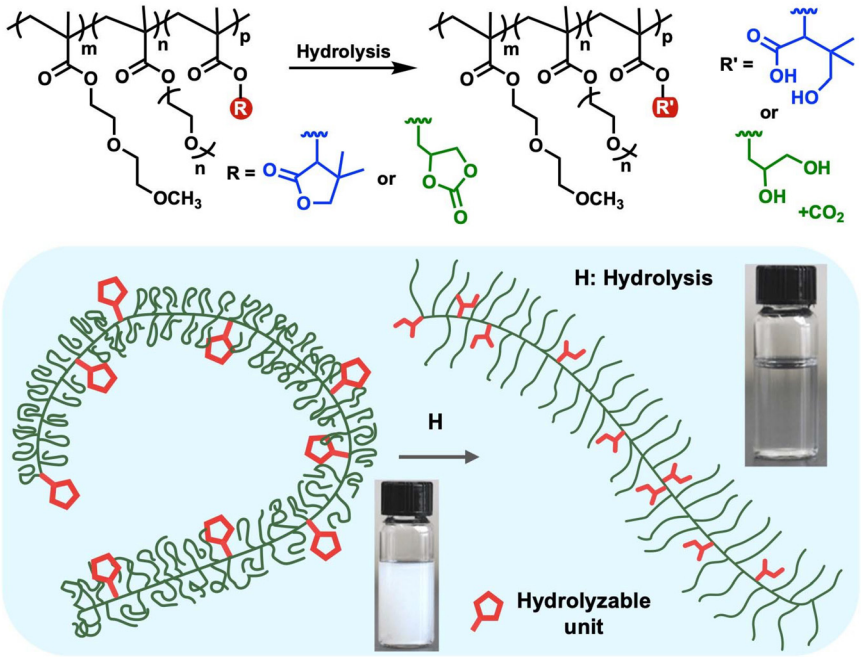

Fig. 1 Lactone and cyclic carbonate functional PEG-methacrylate-based polymers as hydrolyzable and thermoresponsive programmable systems.

DL-Pantolactone (95%, TCI), methacryloyl chloride (Sigma-Aldrich, 97%), triethylamine (TEA, 99%, TCI), 4-(hydroxymethyl)-1,3-dioxolan-2-one (90%, Thermoscientific), 4-cyano-4-(((dodecylthio)carbonothioyl)thio) pentanoic acid (chain transfer agent, CTA, 99%, Boron Molecular) were used as received. *N*-Isopropylacrylamide (NIPAM, ≥98%, TCI) was recrystallized from hexanes and 2,2′-azobis(2-methylpropionitrile) (AIBN, 98%, Sigma-Aldrich) was recrystallized from methanol. For dye release test, Rhodamine B (≥95%, Sigma-Aldrich) and dialysis tubing (Spectrum™ Spectra/Por™ 3, regenerated cellulose, 3.5 kDa MWCO, Fisher Scientific) were used.

2.2. Synthesis of lactone monomer (LMA)

Methacrylate monomer with a hydrolyzable lactone moiety (LMA) was synthesized using the following procedure: A 50 mL Schlenk flask equipped with a magnetic stir bar was charged with DL-pantolactone (511 mg, 3.93 mmol), triethylamine (2.15 mL, 15.36 mmol), and dichloromethane (26 mL). The mixture was cooled to 0 °C and stirred under N_2 for 10 minutes, and then methacryloyl chloride (0.75 mL, 7.68 mmol) was added dropwise, and the reaction mixture was allowed to warm up to room temperature. The reaction mixture was subsequently stirred for 24 hours under N_2 at room temperature. After the completion of the reaction, the solvents were removed under reduced pressure using a rotary evaporator. Ethyl acetate was added to the obtained crude mixture, which resulted in the precipitation of salt. The precipitate was then filtered out, and the filtrate was dried under reduced pressure to obtain the crude mixture. The crude was purified by silica gel column chromatography using a mixture of hexanes and ethyl acetate as the eluent (10 : 1 by volume). Finally, the solvents were removed under reduced pressure to yield the LMA (711 mg, 3.59 mmol, 91% yield) as a colorless oil. The LMA monomer was characterized by ^{1}H, ^{13}C, DEPT (90 and 135), and 2D (HSQC and HMBC) NMR spectroscopy techniques.

2.3. Synthesis of cyclic carbonate monomer (C^2MA)

Methacrylate monomer that has hydrolyzable carbonate (C^2MA)[49–52] was synthesized using the following procedure: a 150 mL Schlenk flask equipped with a magnetic stir bar was charged with 90% pure 4-(hydroxymethyl)-1,3-dioxolan-2-one (1.45 mL, 15.47 mmol), triethylamine (8.6 mL, 61.70 mmol), and dichloromethane (120 mL). The mixture was cooled to 0 °C and stirred under N_2 for 10 minutes, then methacryloyl chloride (3.0 mL, 30.71 mmol) was added, and the reaction mixture was allowed to warm at room temperature. The reaction mixture was subsequently stirred for 24 hours under N_2. After the completion of the reaction, the solvents were removed under reduced pressure. Ethyl acetate was added to the obtained crude product, which resulted in the precipitation of salt. The solid salt residue was then separated by filtration, and the filtrate was evaporated under reduced pressure to obtain the crude product. This crude product was purified by silica gel column chromatography using a 1 : 1 (v/v) mixture of hexanes and ethyl acetate as the eluent. Finally, the solvents were removed under reduced pressure to provide C^2MA (2.65 g, 14.23 mmol, 92% yield) as a colorless oil. The C^2MA monomer was characterized by ^{1}H, ^{13}C, DEPT, and 2D COSY NMR spectroscopy techniques.

2.4. Synthesis of P(DEGMA$_{80}$-*co*-OEGMA$_{10}$-*co*-LMA$_{10}$)

Terpolymer *via* Reversible Addition–Fragmentation Chain Transfer (RAFT) Polymerization. In a 10 mL Schlenk flask equipped with a magnetic stir bar, LMA (90 mg, 0.454 mmol), OEGMA (224 mg, 0.448 mmol), DEGMA (690 mg, 3.67 mmol), CTA (19 mg, 0.047 mmol), AIBN (8 mg, 0.048 mmol), and toluene (2 mL) were added. The reaction mixture was degassed with N_2 sparging and stirred at 70 °C for 13 hours. Polymerization was quenched by exposing the reaction mixture to air under the fume hood while stirring. The crude polymer was purified by precipitation into hexanes. The overall monomer conversion and isolated yield were >90%.

2.5. Synthesis of terpolymer P(DEGMA$_{80}$-*co*-OEGMA$_{10}$-*co*-C^{2}MA$_{10}$) *via* RAFT polymerization

In a 10 mL Schlenk flask equipped with a magnetic stir bar, C^{2}MA (85 mg, 0.456 mmol), OEGMA (228 mg, 0.456 mmol), DEGMA (685 mg, 3.639 mmol), CTA (19 mg, 0.047 mmol), AIBN (8 mg, 0.048 mmol), and toluene (2 mL) were added. The reaction mixture was degassed with N_2 sparging and stirred at 70 °C for 13 hours. Polymerization was quenched by exposing the reaction mixture to air under the fume hood while stirring. The crude polymer was purified by precipitation into hexanes. The overall monomer conversion and isolated yield were >90%.

2.6. Cloud point temperature measurements

The cloud point temperature (T_{cp}) for all terpolymers was determined using 1 wt% solutions in deionized water and phosphate-buffered saline (PBS). Absorption and transmittance spectra for hydrolysis studies were recorded using an Agilent Cary 3500 Peltier UV-Vis spectrophotometer. The temperature was increased at a ramp rate of 0.5 °C min^{-1} while monitoring transmittance at 600 nm, and T_{cp} was defined as the temperature corresponding to 90% transmittance.

2.7. Hydrolysis study of terpolymers

Samples for hydrolysis studies were prepared by dissolving 50 mg of each polymer in 5 mL of deionized water or PBS to obtain 1 wt% solutions. The solutions were maintained at 50 °C on a hot plate for 7 days. After 7 days, the samples were lyophilized and analyzed by ^{1}H NMR spectroscopy. Comparison with the reference spectra revealed no significant structural changes, indicating slow hydrolysis under neutral aqueous conditions. To accelerate hydrolysis, the procedure was repeated using 0.5 M and 1.0 M of HCl and NaOH solutions, enabling comparison of degradation behavior under acidic and basic conditions relative to deionized water and PBS.

2.8. Density functional theory (DFT) calculations

All DFT calculations were performed using Gaussian 16 (Rev. C.02).[53] The PBE0 hybrid functional and the def2-TZVPD basis set was used, D3BJ dispersion correction was included to account for weak interactions. A polarizable continuum model was employed to account for implicit water solvation, while one water molecule was also introduced to further recover the solvation effect. Geometry optimizations were carried out to locate transition states and stationary points. Frequency analysis confirmed the absence of imaginary frequencies for all stationary points and the presence of a single imaginary frequency corresponding to the reaction coordinate for each transition state. Thermodynamic properties were calculated at 298 K and 1 atm.

2.9. Radiofrequency treatment of terpolymers

RF-assisted heating experiments of samples were performed using a custom-built experimental setup. The setup consists of two copper strips on a Teflon block, with one copper strip connected to the inner conductor and the other to the outer conductor of a coaxial cable. A RIGOL DSG836 model signal generator (9 kHz–3 GHz) was used to generate the RF signals, and the corresponding signal was amplified to achieve the desired input power by an RF Amplifier 50W1000D model. RF signals were delivered to the copper strips applicator *via* 50 Ω coaxial cable. Thermal imaging and heating rate data during RF-assisted heating experiments were recorded by FLIR A655sc High-Resolution Science Grade LWIR Camera, and data analysis was performed using FLIR® ResearchIR Recording and Analysis software. To perform heating experiments, 30 μL of solution was added to a quartz glass test tube touching the copper strips in non-contact applicator configuration, whereas in direct-contact configuration, 30 μL of solution was placed directly on the applicator between the copper strips.

2.10. Injectability test of terpolymers

P(DEGMA$_{60}$-*co*-OEGMA$_{10}$-*co*-LMA$_{30}$) (100 mg) was dissolved in a 1-dram vial containing a 1 : 1 (v/v) mixture of H_2O and neon green dye solution to obtain a 10 wt% polymer-dye formulation. Similarly, P(DEGMA$_{60}$-*co*-OEGMA$_{10}$-*co*-C^{2}MA$_{30}$) (100 mg) was dissolved under identical conditions to prepare a corresponding 10 wt% polymer-dye solution. Prior to injection, the prepared agarose gel vials were incubated at 37 °C for 2 hours to ensure thermal equilibration and homogeneity. For injection into the agarose gel matrix, a 1 mL syringe fitted with a 22G needle was employed. In each experiment, 60 μL of the polymer-dye solution was injected into the gel for subsequent observation.

2.11. Dye release test

Dye calibration curves were generated using an Agilent Cary 3500 Peltier UV-Vis spectrophotometer for absorbance measurements and an Agilent Cary Eclipse Fluorescence spectrophotometer for fluorescence measurements across a range of standard Rhodamine B dye concentrations. Dye-release studies were performed in triplicate for each copolymer (30 mol% LMA and 30 mol% C^{2}MA compositions) and for dye-only controls. Polymer samples consisted of 950 μL of 10 wt% polymer in PBS mixed with 50 μL of dye stock solution (1 mg mL^{-1}). Control samples contained 950 μL PBS and 50 μL dye stock solution. Each 1.0 mL formulation was loaded into a dialysis tube, pre-equilibrated at 37 °C for 15 minutes, and subsequently immersed in a 60 mL PBS bath maintained at 37 °C. At predetermined time points, 1.0 mL aliquots were

withdrawn from the external PBS bath for UV-Vis and fluorescence analysis and immediately replaced with 1.0 mL of pre-warmed PBS at 37 °C to maintain constant volume and sink conditions. Dye concentrations were calculated from the calibration equations, and cumulative mass release and percent release (relative to the initial dye loading) were determined.

3. Results and discussion

The objective of this work is to develop thermoresponsive polymer systems featuring side-chain degradable functionality. Upon hydrolysis, these degradable side chains introduce more polar groups, shifting the polymer's overall balance toward a more hydrophilic character. Cyclic esters (lactones) and cyclic carbonates were selected as hydrolyzable ring systems to compare the influence of these two different functional groups, as their ring-opening reactions yield more hydrophilic functionalities than the parent cyclic structures. Hence, we designed and synthesized lactone- and cyclic carbonate-derived monomers that can be incorporated into the polymer backbone as polymerizable, hydrolytically labile units (Schemes S1 and S2). These monomers were copolymerized with ethylene glycol-based monomers using RAFT polymerization[54–56] at varying feed ratios (Schemes S5–S15), enabling tunable thermoresponsive behavior.

The primary aim was to tailor the LCST within the range of room temperature to physiological temperature while maximizing the content of hydrolyzable units. This approach enabled the design of injectable thermoresponsive polymer solutions that undergo a temperature-induced viscosity increase upon injection into the body, followed by time-dependent hydrolysis that gradually enhances hydrophilicity. As the cyclic side chains degrade, they convert to more polar, hydrogen-bonding functionalities, leading to increased polymer swelling and a corresponding decrease in viscosity. This responsive polarity switch facilitates *in situ* transitions, opening new opportunities for applications such as drug delivery systems and smart adhesives that promote tissue regeneration *via* degradation-induced liquefaction. OEGMA (M_n = 500 Da with 8–10 EG units) and DEGMA were chosen as comonomers due to their well-characterized thermoresponsive properties, synthetic flexibility, and extensive use in literature.[24,28] Additionally, OEGMA/DEGMA systems allow for modulation of the LCST over a broad range while accommodating high additional comonomer loadings, enabling precise tuning of the LCST between room and body temperatures. RAFT polymerization offers control over molecular weight, copolymer composition, and dispersity, overcoming the limitations of earlier free radical polymerization methods in the literature.[33,57]

3.1. Synthesis of methacrylate monomer with hydrolyzable lactone and cyclic carbonate derivatives

The methacrylate monomer bearing a lactone functionality (LMA) was synthesized *via* a nucleophilic acyl substitution between hydroxy-functionalized dimethyl-γ-butyrolactone and methacryloyl chloride (Scheme S1). The resulting LMA structure incorporated two functional motifs: (1) a methacrylate moiety enabling reversible-deactivation radical polymerization (RDRP)[58] *via* the RAFT process, and (2) a lactone unit serving as a hydrolyzable domain, designed to impart controlled degradability and tunable thermoresponsive behavior.

The structure of LMA was confirmed by detailed ^{1}H, ^{13}C, and 2D NMR spectroscopy analyses (Fig. S5–S9). In the ^{1}H NMR spectrum, successful esterification was indicated by the downfield shift of the methine (CH) proton (H_a) on the ring adjacent to the ester group (α-carbon on the lactone ring) (from δ ~4.2 to 5.4 ppm), and the appearance of vinylic proton signals at 5.5–6.5 ppm. Notably, the resonance at 4.1 ppm, corresponding to the methylene group (CH_2) of the lactone, remained intact, suggesting that the ring structure was preserved throughout synthesis and purification (Fig. 2A and B). The ^{13}C NMR spectrum exhibited carbonyl resonances at 185 ppm and 171 ppm, consistent with those of the lactone and methacrylate ester carbonyls, respectively. Additionally, a new signal at 75 ppm was assigned to the carbon adjacent to the ester linkage within the cyclic lactone structure, further validating the successful synthesis of the monomer (Fig. S5). The structural assignment of LMA was further corroborated by DEPT and 2D NMR analyses (Fig. S6–S9). Similarly, the methacrylate monomer bearing a cyclic carbonate functionality (C^2MA) was synthesized *via* a nucleophilic acyl substitution between hydroxy-functionalized 4-(hydroxymethyl)-1,3-dioxolan-2-one and methacryloyl chloride (Scheme S2), and the successful synthesis was confirmed by NMR spectroscopy analyses (Fig. 2C, D and Fig. S10–S13). The resulting C^2MA structure also incorporated a polymerizable methacrylate moiety and a hydrolyzable cyclic carbonate unit, enabling controlled degradability and adjustable thermoresponsive properties.

3.2. Designing dual-responsive terpolymer systems

Initially, homopolymers of LMA and C^2MA were prepared *via* RAFT polymerization (Schemes S3 and S4). Monomer conversion was monitored by ^{1}H NMR spectroscopy by the disappearance of vinyl proton resonances and the emergence of broad signals attributed to methylene protons adjacent to ester moieties (Fig. S14 and S15). Near-quantitative monomer conversions were achieved after 14 hours of polymerization reaction. The preservation of the structure during polymerization was confirmed by the absence of new signals associated with ring-opening side reactions and the retention of characteristic signals corresponding to the intact ring structure. As expected, both homopolymers were insoluble in water, prompting the synthesis of copolymers to introduce thermoresponsive behavior.

To develop thermoresponsive polymers with transition temperatures tunable between room and physiological temperatures, a series of copolymers and terpolymers incorporating hydrolyzable comonomers was synthesized *via* RAFT polymerization by systematically varying the monomer feed ratios (Schemes S5–S11). The T_{cp} values of the resulting polymers

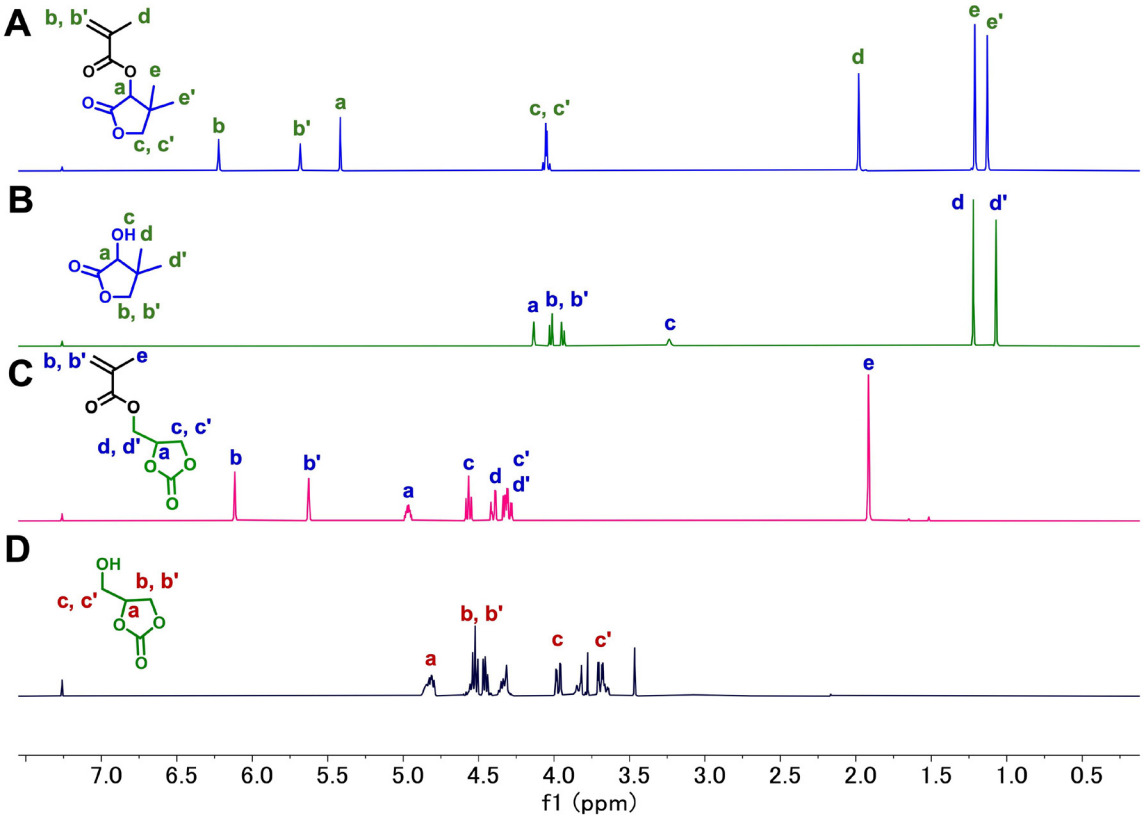

Fig. 2 ^{1}H NMR spectra of (A) LMA monomer, (B) DL-pantolactone, (C) C^{2}MA monomer, and (D) 4-(hydroxymethyl)-1,3-dioxolan-2-one in $CDCl_3$. The starting material in (D) was obtained at 90% purity from the supplier, and the corresponding impurity signals (unassigned) were eliminated following C^{2}MA synthesis and purification.

were determined by turbidity measurements *via* UV-Vis spectroscopy. As anticipated, increasing the LMA or C^{2}MA content, thereby enhancing the overall hydrophobicity within the ethylene glycol-based matrix, led to a decrease in T_{cp} (Tables S1 and S2). A terpolymer strategy was further implemented by incorporating the degradable comonomers (LMA or C^{2}MA) into the OEGMA/DEGMA framework (Schemes S12–S15). This design allowed control over the hydrolyzable comonomer content while maintaining T_{cp} within the physiologically relevant range (25–37 °C) (Table 1). To investigate compositional effects, the feed ratio of degradable comonomers was varied from 10 to 30 mol%. While the feed ratio of the more hydrophilic monomer OEGMA was maintained at 10 mol%, the proportions of the degradable comonomer and DEGMA were varied to obtain terpolymers with the desired T_{cp}. The terpolymer approach enabled direct comparison of not only the type of degradable functionalities but also the effect of composition on thermal behavior.

P(DEGMA$_{80}$-*co*-OEGMA$_{10}$-*co*-LMA$_{10}$) (L10) and P(DEGMA$_{60}$-*co*-OEGMA$_{10}$-*co*-LMA$_{30}$) (L30) were synthesized *via* RAFT polymerization, and their compositions were determined *via* ^{1}H NMR spectroscopy (Fig. S25 and S26). As expected, the terpolymer L10 had a higher T_{cp} than the terpolymer L30 in PBS. While both polymers exhibited narrow molecular weight distributions with dispersity ($Đ$) below 1.5, L30 displayed slightly broader distributions compared to L10. The number average molecular weights (M_n) of the synthesized terpolymers were in the range of 20–50 kDa, as determined by size exclusion chromatography (SEC) (Table 1). This molecular weight range was intentionally targeted to ensure that, following hydrolysis, polymers would remain below the renal clearance threshold (~50–60 kDa), allowing for efficient elimination from the body.[59–61]

Table 1 Cloud point temperature (T_{cp}) and molecular weight data of polymers

Polymer	Feed ratio (DEGMA : OEGMA : M)	Composition (DEGMA : OEGMA : M)	M_n (kDa)	$Đ$	T_{cp} (°C)
L10	80 : 10 : 10	77.9 : 10.3 : 11.6	45.2	1.18	33.4
L30	60 : 10 : 30	57.3 : 9.6 : 33.1	20.5	1.27	28.9
C10	80 : 10 : 10	75.5 : 10.9 : 13.4	20.4	1.25	32.2
C30	60 : 10 : 30	56.5 : 11.9 : 31.6	42.2	1.28	30.1

The conversion profile shows that LMA polymerizes at a slightly faster rate than the combined comonomers (DEGMA + OEGMA) throughout the reaction. At early time points, LMA reaches 34.6% conversion compared to 27.1% for the total comonomer, and this difference persists as the reaction progresses (65.7% *vs.* 54.2% at 2 h; 80.1% *vs.* 71.2% at 3 h) (Table S5 and Fig. S27, S28). Both monomer fractions approach high final conversions after 5 hours reaction time. The parallel increase in conversion suggests effective copolymerization, while the relatively higher LMA conversion indicates slightly greater reactivity under the chosen RAFT conditions. This behavior may lead to subtle compositional drift during polymerization.

The C^2MA monomer was used in the same feed ratios as LMA (10 mol% and 30 mol%) to prepare two sets of terpolymers. We started with 10 mol% of C^2MA, which resulted in a T_{cp} in the targeted range (25–37 °C). To incorporate a higher amount of hydrolyzable units, the feed ratio of C^2MA was increased to 30% which resulted in a decrease in T_{cp}; however, the value remained within the range suitable for injectable applications. P(DEGMA$_{80}$-*co*-OEGMA$_{10}$-*co*-C^2MA_{10}) (C10) and P(DEGMA$_{60}$-*co*-OEGMA$_{10}$-*co*-C^2MA_{30}) (C30) were also synthesized through RAFT polymerization, and their structures were confirmed through ^{1}H NMR spectroscopy (Fig. S29 and S30). The theoretical M_n for these terpolymers was approximately 45 kDa. The experimental M_n of C10 was consistent with the theoretical value, while the M_n of C30 was lower than the expected molecular weight within the desired range (Table 1). A terpolymer of cyclic carbonate with 50 mol% C^2MA incorporation was also synthesized by increasing the molar ratio of C^2MA. The resulting polymer was found to be only partially soluble and did not exhibit a sharp cloud point behavior.

The conversion data indicate that C^2MA polymerizes more rapidly than the combined comonomers (DEGMA + OEGMA) throughout the reaction and at a faster rate than LMA under identical conditions. At early time points, C^2MA reaches 43.2% conversion while the total comonomer conversion remains comparatively low (16.9%), highlighting a pronounced difference in reactivity. This trend persists throughout the polymerization (76.8% *vs.* 56.6% at 2 h; 89.5% *vs.* 75.5% at 3 h), with C^2MA ultimately reaching 96.8% conversion compared to 91.6% for the comonomers after 5 hours (Table S5 and Fig. S31, S32). The consistently higher and faster consumption of C^2MA suggests greater intrinsic reactivity under the RAFT conditions, which may result in early-stage enrichment of C^2MA units and transient compositional drift prior to approaching high overall conversion.

Thermogravimetric analysis (TGA) revealed that the homopolymer of lactone monomer (PLMA) exhibited a decomposition temperature ($T_{d5\%}$, defined at 5% weight loss) of approximately 229 °C. In contrast, the terpolymer L10 displayed a lower $T_{d5\%}$ of 196 °C. This decrease in thermal stability can be attributed to the introduction of the more labile, low glass transition temperature (T_g) PEG-based side chains from DEGMA and OEGMA. Additionally, the reduced proportion of lactone units in the terpolymer matrix diminishes the overall cohesive interactions and thermal rigidity contributed by the lactone segments, thereby lowering the onset of decomposition. Overall, these compositional effects account for the observed decrease in $T_{d5\%}$ of the terpolymer relative to the homopolymer. Further increasing the lactone moiety within the polymer from 10 mol% (L10) to 30 mol% (L30) displayed a similar $T_{d5\%}$ of 195 °C (Fig. 3A).

TGA revealed that the homopolymer of the cyclic carbonate exhibited a $T_{d5\%}$ of 249 °C, highlighting the intrinsic thermal stability imparted by the cyclic carbonate backbone. However, when copolymerized with PEG-based monomers, a substantial decrease in thermal stability was observed. The terpolymer C10 with 80 mol% DEGMA and 10 mol% OEGMA displayed a markedly lower $T_{d5\%}$ of 160 °C. This pronounced reduction is primarily attributed to the high content of DEGMA and OEGMA. Increasing the cyclic carbonate content to 30 mol%, while reducing DEGMA to 60 mol%, resulted in a terpolymer with a higher $T_{d5\%}$ of 205 °C. These observations underscore that the decomposition temperature of these copolymers is governed by a balance between the thermally labile PEG-based side chains and the effect of the cyclic carbonate units. Thus, increasing the fraction of cyclic carbonate effectively enhances the thermal resistance of the terpolymer by reinforcing the polymer backbone and mitigating the susceptibility introduced by the ethylene glycol-rich comonomers (Fig. 3B).

Differential scanning calorimetry (DSC) showed that the terpolymer L30 had a T_g of 8.8 °C (Fig. 3C), while the terpolymer C30 displayed a much lower T_g of −13.1 °C (Fig. 3D) compared to the lactone counterpart. The lactone units introduce more rigidity into the polymer backbone due to their constrained ring structure and stronger dipolar interactions, which restrict chain mobility and raise T_g. In contrast, the cyclic carbonate units possess greater conformational flexibility and lower ring strain, allowing increased mobility of the polymer chain segments.[33,34,62–64]

3.3. Cloud point temperature measurements and hydrolysis study

To evaluate the effect of monomer composition and type on the thermoresponsive behavior of polymers, we initially measured their T_{cp} in DI water. The T_{cp} values of terpolymers were also measured in PBS (Table 1), which consistently exhibited lower T_{cp} values compared to DI water due to a salting-out effect (Table S2).[65,66] PBS contains kosmotropic ions such as Na^+, K^+, and phosphate anions ($H_2PO_4^-$, HPO_4^{2-}), which compete with the ethylene glycol units of the polymer for interacting with water molecules. This competition disrupts hydrogen bonding between the polymer and water, reducing polymer–water interactions and enhancing polymer–polymer associations.[61] As a result, the phase transition occurs at a lower temperature in PBS. This observation is consistent with previous studies on cloud point depression in ethylene glycol-based polymers.[67,68] Additionally, measurements in PBS more accurately reflect the thermoresponsive behavior of the polymers under physiological conditions, due to its representative pH and ionic composition. The terpolymers containing a

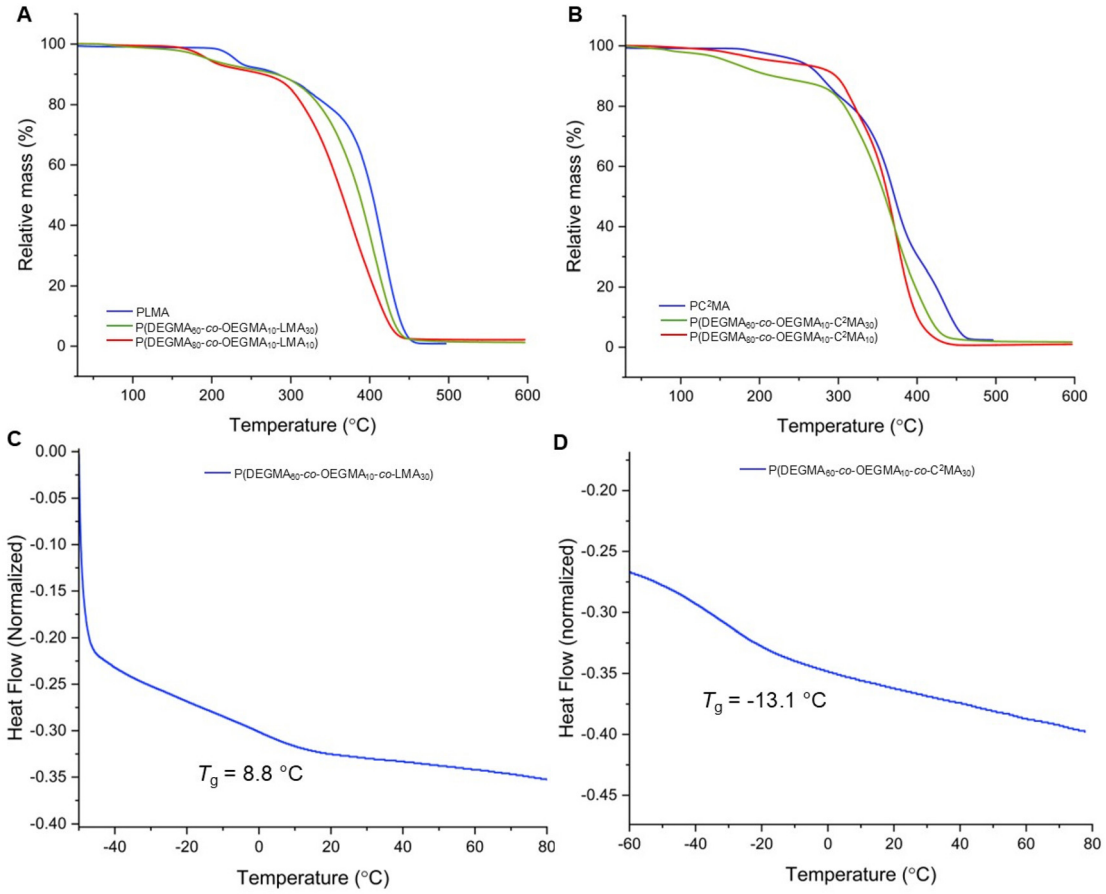

Fig. 3 Thermogravimetric analysis of (A) PLMA and lactone-containing terpolymers; and (B) PC^{2}MA and cyclic carbonate-containing terpolymers. Differential scanning calorimetry traces from the 2nd heating cycle, indicating the glass transition temperatures (T_g); (C) L30 and (D) C30.

higher fraction of hydrolyzable units (L30 and C30) demonstrated a lower T_{cp} than the terpolymers with lower hydrolyzable content (L10 and C10). This trend is consistent with the increased hydrophobic character of LMA and C^{2}MA relative to DEGMA. However, all samples showed a T_{cp} above room temperature and below body temperature, which makes them suitable for injection and operation under physiological conditions (Table 1 and Fig. S68).

To investigate the hydrolytic behavior of the terpolymers, two sets of materials were synthesized incorporating either hydrolyzable lactone or cyclic carbonate side chains. Both monomers feature a five-membered ring with ring strain facilitating hydrolysis in aqueous environments; however, they differ in their chemical structure and degradation kinetics. The lactone unit is directly bonded to the polymer backbone through an ester linkage and contains two geminal methyl groups on the β-carbon, introducing steric hindrance that may slow down hydrolysis. In contrast, the cyclic carbonate moiety is linked to the backbone *via* a bridging methylene group and lacks substituents, resulting in reduced steric hindrance. Additionally, it presents a more hydrophilic nature with a more electrophilic carbonyl. These features collectively lead to faster hydrolysis rates, consistent with the observed kinetic behavior. These differences in hydrolysis profiles are particularly relevant for biomedical applications such as drug delivery systems, where controlled degradation governs release profiles and material clearance.

Hydrolysis of the side chains induces ring opening and formation of hydroxyl and carboxylic acid groups, which increase the overall hydrophilicity of the polymer, improve polymer solubility in aqueous environments, and elevate its T_{cp}. This property is especially desirable for injectable formulations, as it enables slow, tunable swelling, viscosity change, and material clearance following administration. Preliminary hydrolysis studies in DI water showed an opposite trend: instead of the expected T_{cp} increase, the polymers exhibited decreasing T_{cp} values over time (Fig. S60–S66). This behavior was attributed to a decrease in pH of the solution during hydrolysis, which potentially reduced the solubility of the polymer and suppressed further degradation (Fig. S67).

To maintain physiologically relevant conditions and minimize pH fluctuations, the experiments were repeated in PBS. The buffering capacity of PBS stabilized the solution pH, enabling continuous ring opening and formation of hydrophilic moieties. The hydrolysis experiments were limited to 7 days to prevent depletion of the buffer capacity. After 7 days in

PBS, ^{1}H NMR spectra indicated partial hydrolysis (Fig. S33 and S40), and T_{cp} values increased by 3–4 °C relative to pristine samples, reflecting enhanced hydrophilicity. These results suggest that the polymers remain stable yet degradable under physiological conditions over 7 days (Fig. 4). To evaluate complete hydrolysis, accelerated degradation experiments were conducted in 1 M HCl and 1 M NaOH at 50 °C. ^{1}H NMR analysis confirmed complete ring-opening within an hour under these conditions, as evidenced by the disappearance of methine proton signals at 5.2 ppm for the terpolymer L30 and 5.0 ppm for the terpolymer C30 (Fig. S35 and S39).

Kinetic studies were also performed under milder conditions (0.5 M NaOH at 25 °C) to compare hydrolysis kinetics between lactone and cyclic carbonate-containing terpolymers. Under these conditions, C30 hydrolyzed more rapidly than its lactone analogue (Fig. S36 and S40). The methine signal of

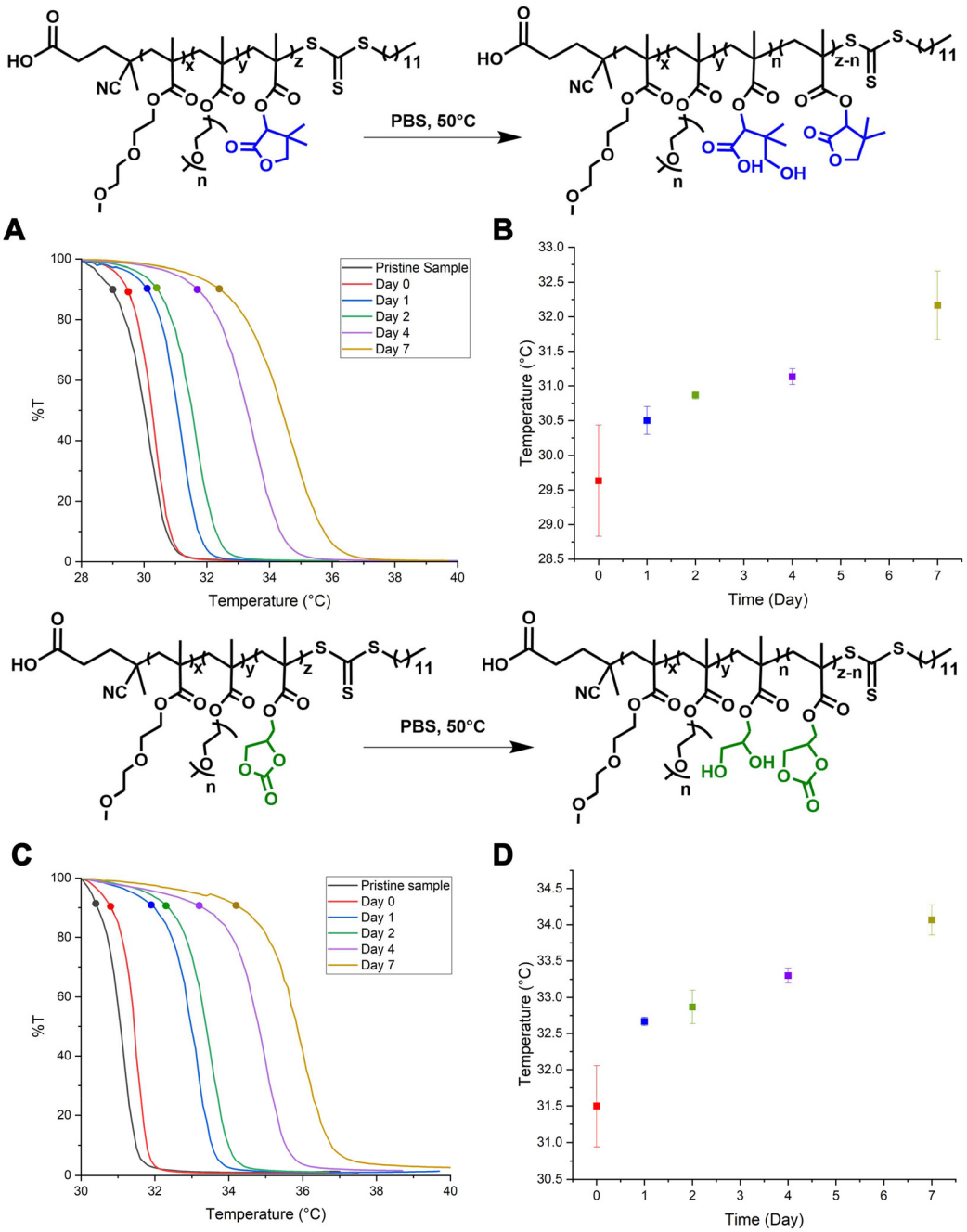

Fig. 4 Time-dependent evolution of cloud point temperature (T_{cp}) resulting from increased polymer hydrophilicity during hydrolysis. Transmittance-temperature profiles for (A) L30 (T_{cp} = 28.9 °C for pristine sample, black line) and (C) C30 (T_{cp} = 30.1 °C for pristine sample, black line). Corresponding scatter plots showing the change in T_{cp} over time during hydrolysis for (B) L30 and (D) C30. Data are presented as mean ± standard deviation from three independent experiments (n = 3).

cyclic carbonate disappeared completely within one hour, while the signal for lactone persisted beyond 8 hours, indicating a slower degradation rate. This difference is attributed to the greater steric hindrance and reduced electrophilicity of the lactone group relative to the cyclic carbonate. FT-IR analysis supported these findings by showing a decrease in ester carbonyl absorption and the emergence of hydroxyl bands post-degradation (Fig. S50–S53). These results highlight how structural and electronic differences in side-chain chemistry can be leveraged to fine-tune hydrolysis rates. Such tunability is critical for designing advanced drug delivery vehicles with time-dependent, predictable degradation and clearance profiles.

3.4. DFT calculations for hydrolysis study

DFT calculations were conducted to examine the hydrolysis mechanisms of lactone and cyclic carbonate side chains (see the SI section S12.11). Hydrolysis proceeds *via* nucleophilic attack by a water-solvated hydroxide anion, forming tetrahedral intermediates that dissociate into carboxylate and alcohol. The rate-limiting step for both lactone and cyclic carbonate hydrolysis is ring-opening alcohol dissociation.[69–71] However, backbone ester hydrolysis is rate-limited by the initial nucleophilic attack due to lower electrophilicity. Lactone hydrolysis is less favorable than carbonate hydrolysis, as steric hindrance from the methyl groups on the lactone ring and the directly attached ester group from the backbone reduces the reaction rate. Additionally, hydrolysis of the backbone ester bond was calculated to be more thermodynamically favorable than that of the lactone ring. It should be noted, however, that these calculations were performed on monomeric units, and factors such as polymer chain length, conformational flexibility, and random coil formation in solution may influence this comparison. In contrast, the cyclic carbonate ring, being less bulky and separated from the ester by a methylene group, facilitates hydrolysis. Gibbs free energy calculations show that carbonate hydrolysis is kinetically favored, and both thermodynamically and kinetically more favorable than ester hydrolysis, possibly due to an intramolecular hydrogen bond between alcohol and carboxylate (Fig. 5).

These results align with experimental observations and highlight the influence of side-chain chemistry on the hydrolysis rate, which can be leveraged to fine-tune degradation behavior in the design of responsive materials. However, these calculations were performed on small molecules, and the behavior of long polymer chains in random coil conformations may differ.

3.5. Potential applications of dual-responsive terpolymers

Preliminary studies were performed to show potential future applications of these dual-responsive polymer systems for injectability, cargo delivery, and external activation. The unique combination of thermoresponsive and hydrolytically degradable functionalities enables these terpolymers to operate under physiological conditions while responding to both internal and external stimuli. To demonstrate this versatility, two representative application areas were explored. First,

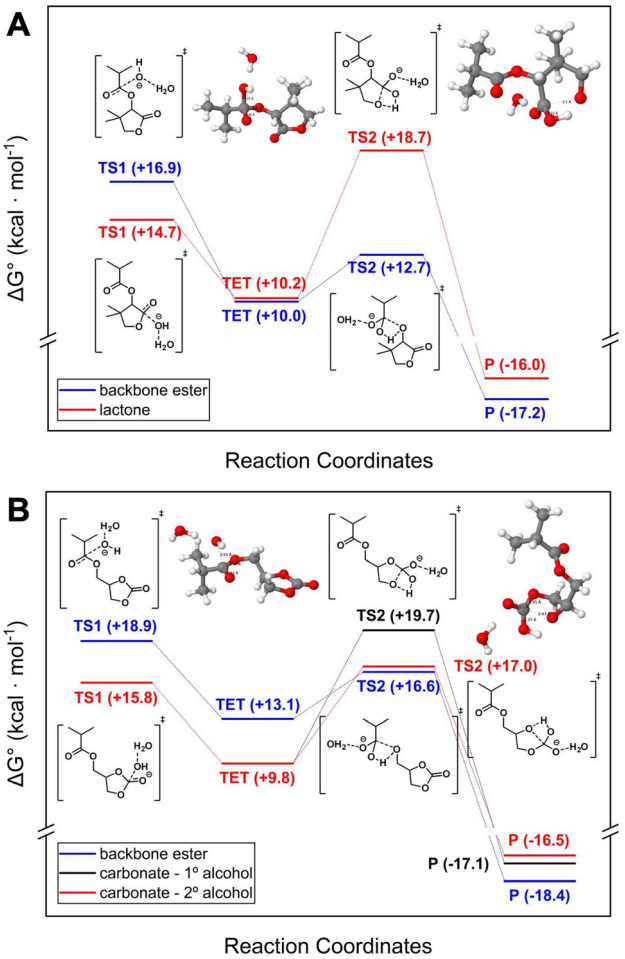

Fig. 5 Gibbs free energy calculated for the alkaline hydrolysis of (A) saturated LMA and (B) saturated C^2MA at 298 K. All calculations were performed at the PBE0-D3BJ/def2-TZVPD[72–76] level of theory with the polarizable continuum model[77] to account for implicit water solvation. The zero-energy reference is set to the sum of the free substrate and the water-solvated hydroxide anion. TS – transition state; TET – tetrahedral intermediate; P – product.

the radiofrequency (RF)-triggered thermal response was examined to evaluate external control over polymer phase transitions and localized heating behavior. Second, the injectability, diffusion characteristics, and dye release of terpolymer solutions were investigated in tissue-mimicking environments and dialysis experiments to assess their suitability for minimally invasive administration and controlled release. These studies establish the foundational performance characteristics of the dual-responsive terpolymers and highlight their promise for next-generation biomedical applications such as on-demand drug delivery, responsive scaffolds, and smart injectable systems.

3.5.1. Radiofrequency triggered thermal transition. We tested the dielectric and thermal response of the prepared samples upon RF field exposure using a custom-built experimental setup (Fig. S2).[78] Dielectric materials contain either permanent or induced dipoles that polarize in response to the

applied electromagnetic field. This polarization occurs through the rotation of dipoles, ionic conduction, or finite displacement of charges, resulting in heat generation, thus dielectric heating of the material.[79] For RF-assisted dielectric heating experiments, we first performed a frequency sweep from 100 to 400 MHz to identify the resonant frequency. At the resonant frequency, the sample experiences minimal resistive losses and exhibits the highest heating rate.[80] We observed that noticeable heating only occurred at 300 MHz within the range that we examined, and therefore, we chose to study the thermal response of the prepared samples at this frequency. Fig. 6 shows the RF heating response of the studied samples with varied input power and RF applicator configuration of direct-contact or non-contact.

Fig. 6A demonstrates a temperature increase of the samples during dielectric heating on a non-contact applicator at 300 MHz and an input power of 50 Watts. A gradual increase in temperature for all samples was observed, with L30 exhibiting the most pronounced increase, achieving a maximum temperature of 76 °C upon five minutes of RF exposure. Thermal images captured by a forward-looking infrared (FLIR) camera of the studied samples at the five-minute mark are shown in Fig. 6B and C for L30 and C30. In contrast to the non-contact applicator, Fig. 6D shows heating rates of the samples using a direct-contact applicator at 300 MHz and an input power of 20 Watts. Accordingly, the direct-contact applicator resulted in a significantly faster heating rate compared to the non-contact configuration for all samples, particularly with an input power of 20 Watts. L30 exhibited the most rapid heating, reaching 105 °C within just 5 seconds of RF-exposure in the direct contact applicator (Fig. 6E) as compared to the non-direct contact applicator, where L30 achieved a maximum of 76 °C after five minutes. These results indicate that the direct contact applicator configuration considerably improved the heating rates under RF fields, likely due to improved energy coupling and reduced heat loss.

The L30 terpolymer consistently exhibited a more rapid temperature increase and reached higher final temperatures under RF fields compared to the C30 terpolymer (Fig. 6F). DI water (blank) and an OEGMA/DEGMA copolymer were used as references. While the blank sample showed no appreciable temperature change under RF stimulation, the OEGMA/DEGMA copolymer displayed a moderate temperature increase, though consistently lower than that of the L30 terpolymer. Interestingly, the C10 terpolymer showed a higher temperature rise and final temperature than the C30 terpolymer, suggesting that increasing the cyclic carbonate content leads to a reduced heating response and slower ramp rate (Fig. S76 and S77). A rapid, localized temperature rise above the T_{cp} under external RF stimulation can induce *in situ* thermal transitions and

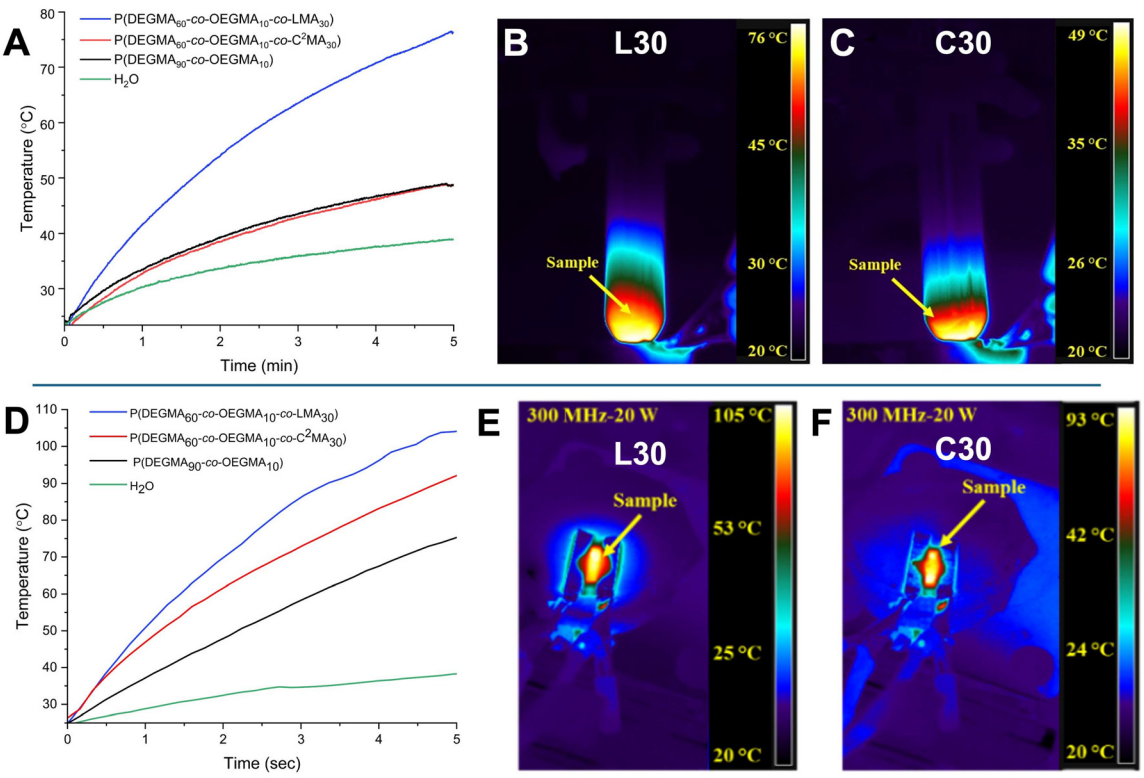

Fig. 6 Temperature change over time for different systems (A) and thermal images captured by FLIR camera at 5-minute mark for L30 (B) and C30 (C) upon RF-assisted dielectric heating on non-contact applicator at 300 MHz and input power of 50 Watt; and temperature change over time for different systems (D) and thermal images captured by FLIR camera at 5-second mark for L30 (E) and C30 (F) upon RF-assisted dielectric heating on direct contact applicator at 300 MHz and input power of 20 Watt.

trigger on-demand hydrolysis of degradable units, leading to increased solubility and reduced viscosity. These preliminary findings highlight the promising potential of RF-triggered heating in terpolymer solutions for future studies.

3.5.2. Injectability test of terpolymers. The pronounced differences in complex viscosity between the terpolymers have important implications for their injectability. Rheological measurements showed that C30 terpolymer solutions exhibited lower viscosities (1–2 Pa s) than the corresponding L30 terpolymer formulations (7–8 Pa s) (Fig. S80–S83), suggesting that C30 can be more easily injected through fine-gauge needles. Complex viscosity obtained from frequency sweep measurements increased for all samples, C30 (10 and 25 wt%) and L30 (10 wt%), when measured above their T_{cp} at 37 °C compared with measurements below T_{cp}, indicating greater resistance to flow. The viscosity exhibits a pronounced increase upon heating through the LCST region, which is attributed to the formation of polymer-rich aggregates resulting from thermally induced phase separation and enhanced hydrophobic interactions that promote interchain association. At 25 °C, the polymer solution displays relatively low viscosity, whereas at 37 °C (above the LCST), the complex viscosity is significantly elevated across the entire frequency range, with an approximately order-of-magnitude increase observed at low frequencies (Fig. S80–S83).

Additionally, frequency and temperature sweep measurements demonstrate that both 10 wt% L30 and C30 in PBS exhibit predominantly viscous behavior, with the loss modulus (G'') consistently exceeding the storage modulus (G') across the tested conditions, indicating viscoelastic liquid characteristics rather than solid-like gel formation. In frequency sweeps, both G' and G'' increase with angular frequency, reflecting typical polymer chain relaxation dynamics. At 37 °C, both terpolymers show substantially higher moduli compared to lower tempera-

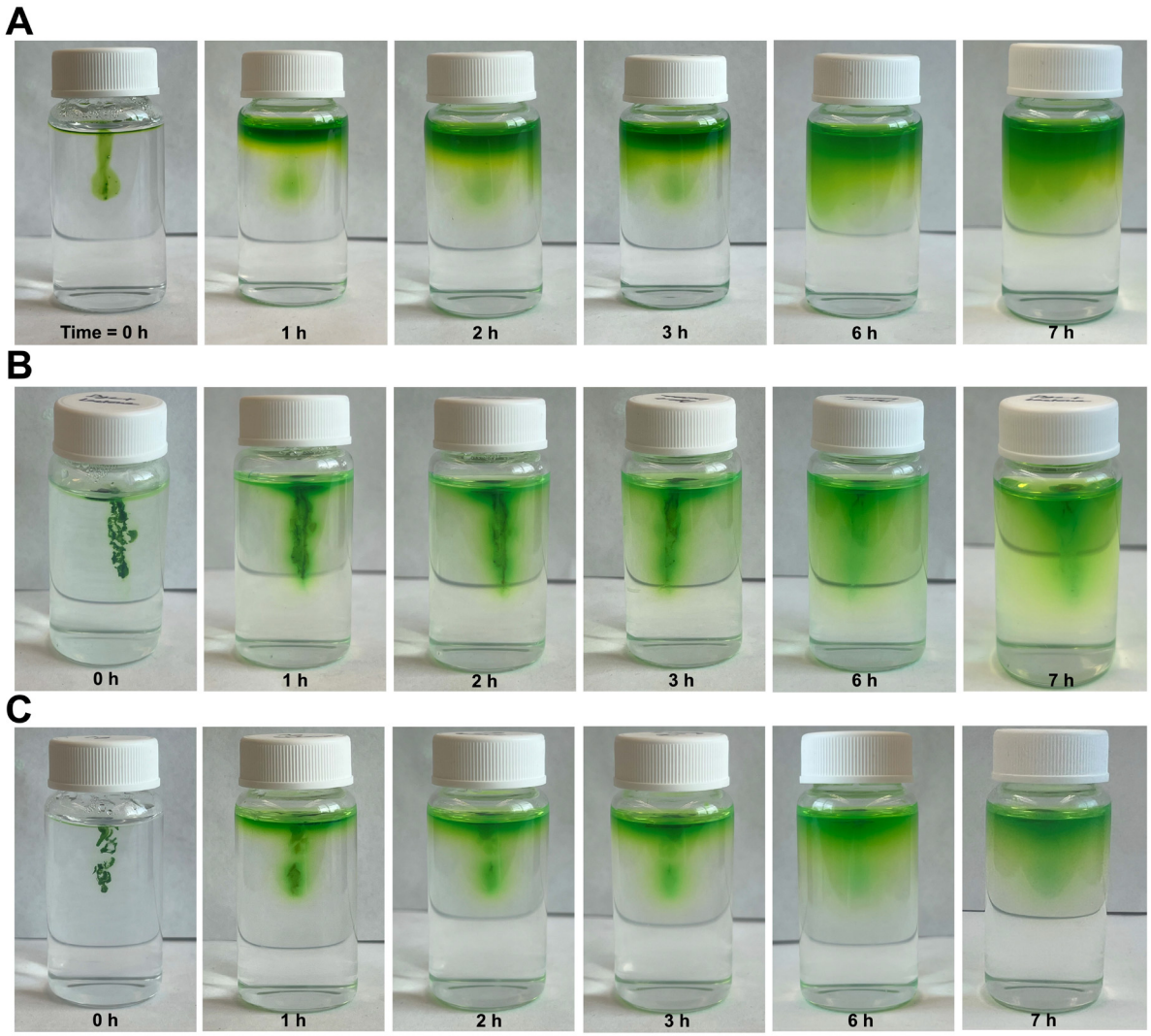

Fig. 7 Injectability test of terpolymers: (A) neon green dye at 37 °C after the injection within the agarose gel at 37 °C with different time intervals, (B) mixture of 10 wt% P(DEGMA$_{60}$-*co*-OEGMA$_{10}$-*co*-LMA$_{30}$) and neon green at 37 °C with different time intervals, and (C) mixture of 10 wt% P(DEGMA$_{60}$-*co*-OEGMA$_{10}$-*co*-C^{2}MA$_{30}$) and neon green at 37 °C with different time intervals.

tures, consistent with enhanced intermolecular interactions near or above their cloud point temperatures. For C30, temperature sweep measurements (25–40 °C, ω = 1 rad s^{-1}) reveal a sharp increase in both G' and G'' above ~35–37 °C, highlighting the onset of LCST-driven aggregation and formation of transient associative domains. Although G'' remains slightly greater than G' in all cases, the marked increase in both moduli at physiological temperature indicates significant thermally induced mechanical reinforcement. Overall, these results confirm that L30 and C30 form temperature-responsive viscoelastic solutions that strengthen near body temperature while maintaining liquid-like behavior without undergoing a full sol–gel transition (Fig. S84–S88). These soft, low-viscosity characteristics with thermal transition and viscosity change near body temperature make these terpolymers promising for injectable systems. Additionally, low viscosity reduces the required injection force and minimizes the risk of shear-induced damage to encapsulated bioactive agents or surrounding tissues. Despite these differences, both terpolymers demonstrated favorable injectability.

To further assess their injectability and potential for controlled release, we selected two representative terpolymers for qualitative evaluation: L30 and C30. Aqueous solutions (10 wt%) of each polymer were injected into a 0.3 wt% agarose gel matrix, pre-formed and incubated at 37 °C to simulate physiological conditions. This tissue-mimicking setup enabled assessment of the polymers' ability to flow through soft matrices and their subsequent behavior over time (Fig. 7). As a control, a neon green dye solution was first injected alone into the agarose gel, which rapidly diffused throughout the matrix. In contrast, when the dye was premixed with either terpolymer solution, diffusion was markedly slower. This reduced dispersion is attributed to the polymer networks entrapping the dye molecules and modulating their release.

The images in Fig. 7 show a time-lapse comparison of injectability and diffusion behavior for three different systems (Fig. 7A only dye, Fig. 7B dye mixture with terpolymer L30, and Fig. 7C dye mixture with terpolymer C30) over a 7-hour period using a neon green dye as a tracer. Only the dye system exhibited the most streamlined and easy injectability, with the dye entering cleanly; however, diffusing symmetrically upward and accumulating at the top. Over time, a clear diffusion front formed, and by 7 hours, the dye was dispersed only in the upper portion of the vial. In contrast, the L30 + dye system demonstrated relatively harder injectability through a 22G needle, with the dye-polymer system initially appearing as clumped aggregates, suggesting a more viscous or semi-solid nature. The diffusion was slower, although slightly irregular, with streaking and less vertical movement during the 7-hour period. This behavior points to a formulation that resists dispersion and may be suited for localized or depot-based delivery applications. The C30 + dye system displayed intermediate characteristics: while some clumping was observed during injection, the dye dispersed more uniformly than in the L30 + dye system. Over time, the dye formed a broader but slightly uneven gradient, reflecting moderate viscosity and improved diffusion compared to the L30 + dye system, probably due to the faster hydrolysis behavior. Overall, while the L30 + dye

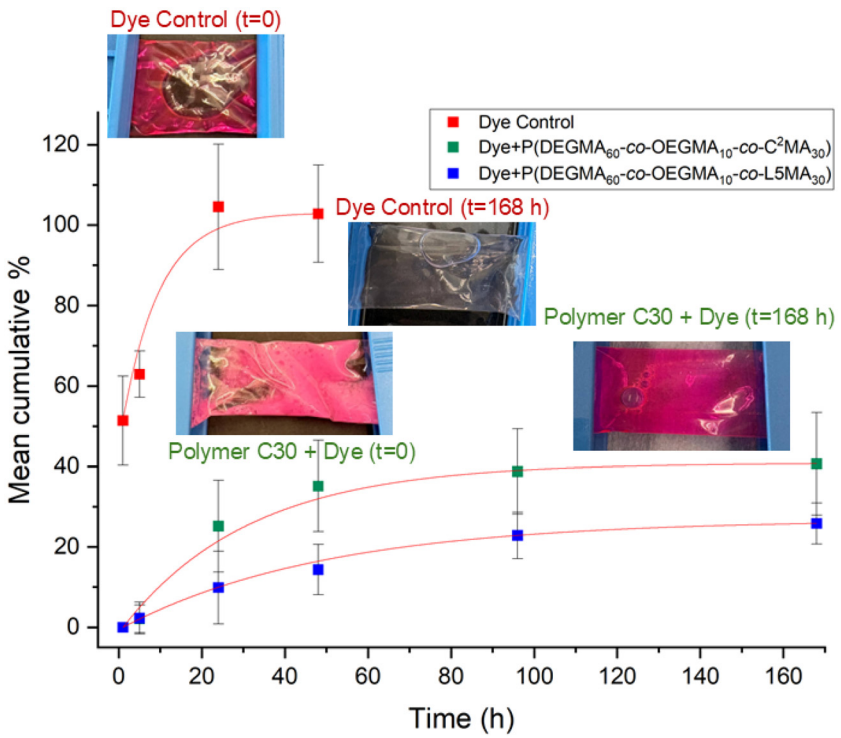

Fig. 8 Dye release study over time. Data represent the mean ± SD of three independent experiments (n = 3).

system suggested a more viscous and localized release profile, the C30 + dye system offered a balance between injectability and controlled release. These results confirm that both terpolymers are readily injectable and can sustain the release of encapsulated small molecules, highlighting their potential as injectable scaffolds for controlled delivery in biomedical applications.

3.5.3. Dye release test. To assess the suitability of these materials as sustained drug-delivery platforms, we quantified dye release from polymer-loaded samples and compared the profiles to dye-only controls under identical dialysis conditions. As expected for a freely diffusing small molecule, the dye-only controls exhibited a rapid early release and approached near-complete release within the first day. In contrast, dye release from the polymer formulations was markedly slower, indicating that polymer-dye interactions and restricted diffusion within the polymer-rich phase delayed transport to the external bath. The release profiles were biphasic, with a higher initial release rate during the first hours followed by a slower, sustained release after day 1 (Fig. 8).

Comparing the two polymer compositions, L30 released dye more slowly than C30 across the study period, consistent with stronger cargo retention and/or lower effective diffusivity in the L30 matrix under these conditions. Overall, these results demonstrate that the polymers prolong dye retention relative to free dye and enable sustained release at 37 °C, supporting their potential as controlled-release carriers (Fig. 8).

Over the 7-day release study, both polymers showed sustained release of the loaded dye, with incomplete release over the study window. By day 7, C30 released ~40% and L30 released ~21% of the initial dye. The observed partial, time-dependent release is almost consistent with controlled-release behavior commonly reported for polymer-based carrier systems, although direct quantitative comparison across studies is limited by differences in cargo identity, loading, and experimental conditions.[81,82]

4. Conclusions

In this work, we developed a new class of thermoresponsive and hydrolytically degradable PEG-based terpolymers incorporating lactone or cyclic carbonate side chains to enable injectable formulations with tunable thermal transitions and controlled degradation profiles. Using RAFT polymerization, we systematically varied comonomer composition to precisely modulate the LCST (25–37 °C), viscosity, thermal stability, and hydrolysis kinetics. Structure–property analyses revealed that the identity and content of degradable side groups govern thermal response, degradation rate, and rheological performance. Notably, cyclic carbonate–containing terpolymers exhibited lower glass transition temperatures, reduced viscosity, and faster hydrolysis compared to lactone analogues, making them more suitable for minimally invasive, resorbable applications. Both systems demonstrated LCST-type transitions near physiological temperature and hydrolysis-driven shifts in T_{cp}, enabling programmable degradation behavior. Rheological and injectability studies confirmed thermally induced sol–gel transitions and shear-thinning characteristics compatible with clinical injection forces, while RF stimulation provided remote, on-demand control of phase transitions. Collectively, these multifunctional terpolymers represent a versatile and programmable platform for next-generation injectable biomaterials with dual responsiveness, tunable degradation, and customizable mechanical and thermal properties for applications in drug delivery, tissue engineering, and adaptive biomedical devices.

Author contributions

Maryam Behzad Khoshgoee: writing – original draft, visualization, validation, methodology, formal analysis, data curation. Mithun Kumar Debnath: writing – original draft, visualization, validation, methodology, formal analysis, data curation. Griffin Pardo: writing – review & editing, methodology, validation, formal analysis. Yichun Yuan: writing – original draft, methodology, validation, formal analysis. Muhammad Zeeshan: writing – original draft, methodology, validation, formal analysis. Erqian Mao: writing – original draft, software, validation, methodology, formal analysis. Thomas G. Gray: writing – review & editing, supervision, funding acquisition. Burcu Gurkan: writing – review & editing, supervision, funding acquisition. Matthew J. Bertin: formal analysis, writing – review & editing. Metin Karayilan: writing – original draft, writing – review & editing, supervision, resources, methodology, conceptualization.

Conflicts of interest

There are no conflicts to declare.

Data availability

The data supporting this article have been included as part of the supplementary information (SI). Supplementary information: detailed descriptions of the materials, equipment, and experimental procedures; the synthesis of hydrolyzable monomers (lactone and cyclic carbonate), homopolymers, copolymers, and terpolymers *via* RAFT polymerization; information on the determination of polymer composition using NMR, cloud point temperature (T_{cp}) measurements, hydrolysis studies, kinetics, and rheological analyses; results from radio-frequency treatment of terpolymers, injectability tests, and various characterization methods such as NMR, FT-IR, TGA, DSC, GPC, and UV-vis spectroscopy; DFT calculations for understanding the hydrolysis mechanisms of the terpolymers. See DOI: https://doi.org/10.1039/d5lp00379b.

Acknowledgements

This work is supported by Case Western Reserve University (CWRU) and Expanding Horizons Initiative (EHI) at CWRU and American Chemical Society (ACS) Doctoral New Investigator (DNI) grant (PRF# DNI68078-DNI7). B. G. acknowledges funding from U.S. Department of Energy, Office of Science, Basic Energy Sciences under award number DE-SC0026299 for the development of RF applicators and dielectric heating studies. Computations were supported by the U.S. Army Research Office, contract W911NF2510003 to T. G. G.

References

1 M. Wei, Y. Gao, X. Li and M. J. Serpe, Stimuli-responsive polymers and their applications, *Polym. Chem.*, 2017, **8**(1), 127–143, DOI: 10.1039/C6PY01585A.
2 F. Liu and M. W. Urban, Recent advances and challenges in designing stimuli-responsive polymers, *Prog. Polym. Sci.*, 2010, **35**(1), 3–23, DOI: 10.1016/j.progpolymsci.2009.10.002.
3 M. A. C. Stuart, W. T. S. Huck, J. Genzer, M. Müller, C. Ober, M. Stamm, G. B. Sukhorukov, I. Szleifer, V. V. Tsukruk, M. Urban, *et al.*, Emerging applications of stimuli-responsive polymer materials, *Nat. Mater.*, 2010, **9**(2), 101–113, DOI: 10.1038/nmat2614.
4 C. D. L. H. Alarcón, S. Pennadam and C. Alexander, Stimuli responsive polymers for biomedical applications, *Chem. Soc. Rev.*, 2005, **34**(3), 276–285, DOI: 10.1039/B406727D.
5 P. Theato, B. S. Sumerlin, R. K. O'Reilly and T. H. Epps, III, Stimuli responsive materials, *Chem. Soc. Rev.*, 2013, **42**(17), 7055–7056, DOI: 10.1039/C3CS90057F.
6 P. Rajagopal, G. R. Jayandharan and U. Maheswari Krishnan, Polyketal-based, nanocarriers: A new class of stimuli-responsive delivery systems for therapeutic applications, *Eur. Polym. J.*, 2022, **173**, 111290, DOI: 10.1016/j.eurpolymj.2022.111290.
7 Y. Yuan, K. Raheja, N. B. Milbrandt, S. Beilharz, S. Tene, S. Oshabaheebwa, U. A. Gurkan, A. C. S. Samia and M. Karayilan, Thermoresponsive polymers with LCST transition: synthesis, characterization, and their impact on biomedical frontiers, *RSC Appl. Polym.*, 2023, **1**(2), 158–189, DOI: 10.1039/D3LP00114H.
8 M. T. Cook, P. Haddow, S. B. Kirton and W. J. McAuley, Polymers Exhibiting Lower Critical Solution Temperatures as a Route to Thermoreversible Gelators for Healthcare, *Adv. Funct. Mater.*, 2021, **31**(8), 2008123, DOI: 10.1002/adfm.202008123.
9 S. Dai, P. Ravi and K. C. Tam, pH-Responsive polymers: synthesis, properties and applications, *Soft Matter*, 2008, **4**(3), 435–449, DOI: 10.1039/B714741D.
10 V. K. Kannaujiya, W. Ling, C. H. Wang, J. Zhang and C. Boyer, Fabrication of pH-responsive smart films from P(3HB-co-4HB) and acetal-modified dextran for controlled drug release, *Eur. Polym. J.*, 2025, **240**, 114327, DOI: 10.1016/j.eurpolymj.2025.114327.
11 F. D. Jochum, L. zur Borg, P. J. Roth and P. Theato, Thermo- and Light-Responsive Polymers Containing Photoswitchable Azobenzene End Groups, *Macromolecules*, 2009, **42**(20), 7854–7862, DOI: 10.1021/ma901295f.
12 V. Yesilyurt, M. J. Webber, E. A. Appel, C. Godwin, R. Langer and D. G. Anderson, Injectable Self-Healing Glucose-Responsive Hydrogels with pH-Regulated Mechanical Properties, *Adv. Mater.*, 2016, **28**(1), 86–91, DOI: 10.1002/adma.201502902.
13 D. H.-C. Chou, M. J. Webber, B. C. Tang, A. B. Lin, L. S. Thapa, D. Deng, J. V. Truong, A. B. Cortinas, R. Langer and D. G. Anderson, Glucose-responsive insulin activity by covalent modification with aliphatic phenylboronic acid conjugates, *Proc. Natl. Acad. Sci. U. S. A.*, 2015, **112**(8), 2401–2406, DOI: 10.1073/pnas.1424684112.
14 C. E. Callmann, C. V. Barback, M. P. Thompson, D. J. Hall, R. F. Mattrey and N. C. Gianneschi, Therapeutic Enzyme-Responsive Nanoparticles for Targeted Delivery and Accumulation in Tumors, *Adv. Mater.*, 2015, **27**(31), 4611–4615, DOI: 10.1002/adma.201501803.
15 D. Roy, W. L. A. Brooks and B. S. Sumerlin, New directions in thermoresponsive polymers, *Chem. Soc. Rev.*, 2013, **42**(17), 7214–7243, DOI: 10.1039/C3CS35499G.
16 F. Doberenz, K. Zeng, C. Willems, K. Zhang and T. Groth, Thermoresponsive polymers and their biomedical application in tissue engineering – a review, *J. Mater. Chem. B*, 2020, **8**(4), 607–628, DOI: 10.1039/C9TB02052G.
17 N. Vanparijs, L. Nuhn and B. G. De Geest, Transiently thermoresponsive polymers and, their applications in biomedicine, *Chem. Soc. Rev.*, 2017, **46**(4), 1193–1239, DOI: 10.1039/C6CS00748A.
18 Y.-J. Kim and Y. T. Matsunaga, Thermo-responsive polymers and their application as smart biomaterials, *J. Mater. Chem. B*, 2017, **5**(23), 4307–4321, DOI: 10.1039/C7TB00157F.
19 S. Beilharz, M. K. Debnath, D. Vinella, A. J. Shoffstall and M. Karayilan, Advances in Injectable Polymeric Biomaterials and Their Contemporary Medical Practices, *ACS Appl. Bio Mater.*, 2024, **7**(12), 8076–8101, DOI: 10.1021/acsabm.4c01001.
20 Y. Yuan, S. Beilharz, H. R. Everson, N. Nupnar, M. K. Debnath, D. Vinella, J. M. Urueña, F. H. Örge, M. J. A. Hore, D. Mathur, *et al.*, Injectable Fluorescent Bottlebrush Polymers for Interventional Procedures and Biomedical Imaging, *Biomacromolecules*, 2025, **26**(2), 1234–1250, DOI: 10.1021/acs.biomac.4c01550.
21 M. Kumar Debnath, M. Behzad Khoshgoee, G. Pardo, M. Zeeshan, E. Mao, Y. Yuan, T. Gray, B. Gurkan, M. J. Bertin and M. Karayilan, Multi-Responsive Polymers with Degradable Side-Chain Functionality, *ChemRxiv*, 2025, preprint, 2025(1201). DOI: DOI: 10.26434/chemrxiv-2025-n1bqn.
22 N. A. Shaibie, N. A. Ramli, N. D. F. Mohammad Faizal, T. Srichana and M. C. I. Mohd Amin, Poly(N-isopropylacrylamide)-Based Polymers: Recent Overview for the Development of Temperature-Responsive Drug Delivery

and Biomedical Applications, *Macromol. Chem. Phys.*, 2023, **224**(20), 2300157, DOI: 10.1002/macp.202300157.

23 S. Ashraf, H.-K. Park, H. Park and S.-H. Lee, Snapshot of phase transition in thermoresponsive hydrogel PNIPAM: Role in drug delivery and tissue engineering, *Macromol. Res.*, 2016, **24**(4), 297–304, DOI: 10.1007/s13233-016-4052-2.

24 J.-F. Lutz, Thermo-Switchable Materials Prepared Using the OEGMA-Platform, *Adv. Mater.*, 2011, **23**(19), 2237–2243, DOI: 10.1002/adma.201100597.

25 K. Raheja, A. Shorin, D. G. Gagnon, R. Lutz, M. B. Hasan, M. Singh, S. M. Parker, S. Morozova and M. Karayilan, Thermoresponsive and Flow Behavior of Hyperbranched Polymers From ATRP Inimer, *J. Polym. Sci.*, 2025, **63**(23), 5115–5130, DOI: 10.1002/pol.20250830.

26 R. Hoogenboom and H. Schlaad, Thermoresponsive poly(2-oxazoline)s, polypeptoids, and polypeptides, *Polym. Chem.*, 2017, **8**(1), 24–40, DOI: 10.1039/C6PY01320A.

27 B. D. Monnery and R. Hoogenboom, Thermoresponsive hydrogels formed by poly(2-oxazoline) triblock copolymers, *Polym. Chem.*, 2019, **10**(25), 3480–3487, DOI: 10.1039/C9PY00300B.

28 J.-F. Lutz, Ö. Akdemir and A. Hoth, Point by Point Comparison of Two Thermosensitive Polymers Exhibiting a Similar LCST: Is the Age of Poly(NIPAM) Over?, *J. Am. Chem. Soc.*, 2006, **128**(40), 13046–13047, DOI: 10.1021/ja065324n.

29 Z. Cui, B. H. Lee and B. L. Vernon, New Hydrolysis-Dependent Thermosensitive Polymer for an Injectable Degradable System, *Biomacromolecules*, 2007, **8**(4), 1280–1286, DOI: 10.1021/bm061045g.

30 B. F. L. Lai, Y. Zou, D. E. Brooks and J. N. Kizhakkedathu, The influence of poly-N-[(2,2-dimethyl-1,3-dioxolane) methyl]acrylamide on fibrin polymerization, cross-linking and clot structure, *Biomaterials*, 2010, **31**(22), 5749–5758, DOI: 10.1016/j.biomaterials.2010.03.076.

31 S. Jana, B. Daelman, M. Purino and R. Hoogenboom, Thermoresponsive Poly(2-Oxazoline)s with pH-Degradable Acetal Side Chains as Potential Drug Delivery Vehicles, *Macromolecules*, 2025, **58**(12), 6098–6110, DOI: 10.1021/acs.macromol.5c00771.

32 E. Henderson, B. H. Lee, Z. Cui, R. McLemore, T. A. Brandon and B. L. Vernon, In vivo evaluation of injectable thermosensitive polymer with time-dependent LCST, *J. Biomed. Mater. Res., Part A*, 2009, **90A**(4), 1186–1197, DOI: 10.1002/jbm.a.32179.

33 Z. Cui, B. H. Lee, C. Pauken and B. L. Vernon, Manipulating degradation time in a N-isopropylacrylamide-based co-polymer with hydrolysis-dependent LCST, *J. Biomater. Sci., Polym. Ed.*, 2010, **21**(6–7), 913–926.

34 Z. Cui, B. H. Lee, C. Pauken and B. L. Vernon, Degradation, cytotoxicity, and biocompatibility of NIPAAm-based thermosensitive, injectable, and bioresorbable polymer hydrogels, *J. Biomed. Mater. Res., Part A*, 2011, **98A**(2), 159–166, DOI: 10.1002/jbm.a.33093.

35 K. Wang, Q. Liu, G. Lu, Y. Zhang, Y. Zhou, S. Chen, Q. Ma, G. Liu and Y. Zeng, Acid-Labile Temperature-Responsive Homopolymers and a Diblock Copolymer Bearing the Pendent Acetal Group, *Macromolecules*, 2021, **54**(8), 3725–3734, DOI: 10.1021/acs.macromol.1c00157.

36 J. Sun, Y. Dong, L. Cao, X. Wang, S. Wang and Y. Hu, Highly Efficient Chemoselective Deprotection of O, O-Acetals and O,O-Ketals Catalyzed by Molecular Iodine in Acetone, *J. Org. Chem.*, 2004, **69**(25), 8932–8934, DOI: 10.1021/jo0486239.

37 P. Saravanan, M. Chandrasekhar, R. Vijaya Anand and V. K. Singh, An efficient method for deprotection of acetals, *Tetrahedron Lett.*, 1998, **39**(19), 3091–3092, DOI: 10.1016/S0040-4039(98)00366-9.

38 S. Mitragotri, Healing sound: the use of ultrasound in drug delivery and other therapeutic applications, *Nat. Rev. Drug Discovery*, 2005, **4**(3), 255–260, DOI: 10.1038/nrd1662.

39 B. A. Versaw, T. Zeng, X. Hu and M. J. Robb, Harnessing the Power of Force: Development of Mechanophores for Molecular Release, *J. Am. Chem. Soc.*, 2021, **143**(51), 21461–21473, DOI: 10.1021/jacs.1c11868.

40 Y. Yao, M. E. McFadden, S. M. Luo, R. W. Barber, E. Kang, A. Bar-Zion, C. A. B. Smith, Z. Jin, M. Legendre, B. Ling, *et al.*, Remote control of mechanochemical reactions under physiological conditions using biocompatible focused ultrasound, *Proc. Natl. Acad. Sci. U. S. A.*, 2023, **120**(39), e2309822120, DOI: 10.1073/pnas.2309822120.

41 T. Zeng, L. A. Ordner, P. Liu and M. J. Robb, Multimechanophore Polymers for Mechanically Triggered Small Molecule Release with Ultrahigh Payload Capacity, *J. Am. Chem. Soc.*, 2024, **146**(1), 95–100, DOI: 10.1021/jacs.3c11927.

42 Y. Shi, C. Ma, Y. Du and G. Yu, Microwave-responsive polymeric core–shell microcarriers for high-efficiency controlled drug release, *J. Mater. Chem. B*, 2017, **5**(19), 3541–3549, DOI: 10.1039/C7TB00235A.

43 J. Thévenot, H. Oliveira, O. Sandre and S. Lecommandoux, Magnetic responsive polymer composite materials, *Chem. Soc. Rev.*, 2013, **42**(17), 7099–7116, DOI: 10.1039/C3CS60058K.

44 M. M. Caruso, D. A. Davis, Q. Shen, S. A. Odom, N. R. Sottos, S. R. White and J. S. Moore, Mechanically-Induced Chemical Changes in Polymeric Materials, *Chem. Rev.*, 2009, **109**(11), 5755–5798, DOI: 10.1021/cr9001353.

45 Y. Lin, T. B. Kouznetsova and S. L. Craig, Mechanically Gated Degradable Polymers, *J. Am. Chem. Soc.*, 2020, **142**(5), 2105–2109, DOI: 10.1021/jacs.9b13359.

46 S. Namathoti, V. M. Ravindra kumar and P. S. Rama Sreekanth, A review on progress in magnetic, microwave, ultrasonic responsive Shape-memory polymer composites, *Mater. Today: Proc.*, 2022, **56**, 1182–1191, DOI: 10.1016/j.matpr.2021.11.151.

47 D. C. Webster, Cyclic carbonate functional polymers and their applications, *Prog. Org. Coat.*, 2003, **47**(1), 77–86, DOI: 10.1016/S0300-9440(03)00074-2.

48 F. D. Bobbink, F. Menoud and P. J. Dyson, Synthesis of Methanol and Diols from CO2 via Cyclic Carbonates under Metal-Free, Ambient Pressure, and Solvent-Free Conditions, *ACS Sustainable Chem. Eng.*, 2018, **6**(9), 12119–12123, DOI: 10.1021/acssuschemeng.8b02453.

49 H. E. Katz, Preparation of soluble poly(carbonyldioxyglyceryl methacrylate), *Macromolecules*, 1987, **20**(8), 2026–2027, DOI: 10.1021/ma00174a057.
50 S. Jana, A. Parthiban and C. L. L. Chai, Transparent, flexible and highly conductive ion gels from ionic liquid compatible cyclic carbonate network, *Chem. Commun.*, 2010, **46**(9), 1488–1490, DOI: 10.1039/B921517D.
51 N. Yadav, F. Seidi, S. Del Gobbo, V. D'Elia and D. Crespy, Versatile functionalization of polymer nanoparticles with carbonate groups via hydroxyurethane linkages, *Polym. Chem.*, 2019, **10**(26), 3571–3584, DOI: 10.1039/C9PY00597H.
52 R. Mahadev Patil, A. A. Ghanwat, S. Ganugapati and R. Gnaneshwar, Synthesis and Characterization of Four-Arm Star Poly(ε-caprolactone)-Block-Poly(cyclic-carbonate methacrylate) Copolymers by Combining Ring-Opening Polymerization With Atom Transfer Radical Polymerization, *J. Macromol. Sci., Part A:Pure Appl. Chem.*, 2015, **52**(2), 114–123, DOI: 10.1080/10601325.2015.980761.
53 *Gaussian 16 Rev. C.01*, Wallingford, CT, 2016.
54 J. Chiefari, Y. K. Chong, F. Ercole, J. Krstina, J. Jeffery, T. P. T. Le, R. T. A. Mayadunne, G. F. Meijs, C. L. Moad, G. Moad, *et al.*, Living Free-Radical Polymerization by Reversible Addition–Fragmentation Chain Transfer: The RAFT Process, *Macromolecules*, 1998, **31**(16), 5559–5562, DOI: 10.1021/ma9804951.
55 G. Moad, Y. K. Chong, A. Postma, E. Rizzardo and S. H. Thang, Advances in RAFT polymerization: the synthesis of polymers with defined end-groups, *Polymer*, 2005, **46**(19), 8458–8468, DOI: 10.1016/j.polymer.2004.12.061.
56 G. Moad, E. Rizzardo and S. H. Thang, Radical addition–fragmentation chemistry in polymer synthesis, *Polymer*, 2008, **49**(5), 1079–1131, DOI: 10.1016/j.polymer.2007.11.020.
57 Z. Cui, B. H. Lee, C. Pauken and B. L. Vernon, Degradation, cytotoxicity, and biocompatibility of NIPAAm–based thermosensitive, injectable, and bioresorbable polymer hydrogels, *J. Biomed. Mater. Res., Part A*, 2011, **98**(2), 159–166.
58 N. Corrigan, K. Jung, G. Moad, C. J. Hawker, K. Matyjaszewski and C. Boyer, Reversible-deactivation radical polymerization (Controlled/living radical polymerization): From discovery to materials design and applications, *Prog. Polym. Sci.*, 2020, **111**, 101311, DOI: 10.1016/j.progpolymsci.2020.101311.
59 Y. Chen, W. Tang, F. Yu, Y. Xie, L. Jaramillo, H.-S. Jang, J. Li, B. J. Padanilam and D. Oupický, Determinants of preferential renal accumulation of synthetic polymers in acute kidney injury, *Int. J. Pharm.*, 2019, **568**, 118555, DOI: 10.1016/j.ijpharm.2019.118555.
60 F. Rypáček, J. Drobník, V. Chmelař and J. Kálal, The renal excretion and retention of macromolecules, *Pflugers Arch.*, 1982, **392**(3), 211–217, DOI: 10.1007/BF00584298.
61 Y. Zhang, S. Furyk, D. E. Bergbreiter and P. S. Cremer, Specific Ion Effects on the Water Solubility of Macromolecules: PNIPAM and the Hofmeister Series, *J. Am. Chem. Soc.*, 2005, **127**(41), 14505–14510, DOI: 10.1021/ja0546424.
62 Y. Wang, Y. Xia, Z. Hua, C. Zhang and X. Zhang, Chemoselective ring-opening copolymerization of five-membered cyclic carbonates and carbonyl sulfide toward poly(thioether)s, *Polym. Chem.*, 2022, **13**(37), 5397–5403, DOI: 10.1039/D2PY01014C.
63 W. Saiyasombat, R. Molloy, T. M. Nicholson, A. F. Johnson, I. M. Ward and S. Poshyachinda, Ring strain and polymerizability of cyclic esters, *Polymer*, 1998, **39**(23), 5581–5585, DOI: 10.1016/S0032-3861(97)10370-6.
64 A. Bodaghi, An overview on the recent developments in reactive plasticizers in polymers, *Polym. Adv. Technol.*, 2020, **31**(3), 355–367, DOI: 10.1002/pat.4790.
65 R. Sadeghi and F. Jahani, Salting-In and Salting-Out of Water-Soluble Polymers in Aqueous Salt Solutions, *J. Phys. Chem. B*, 2012, **116**(17), 5234–5241, DOI: 10.1021/jp300665b.
66 M. J. Hey, D. P. Jackson and H. Yan, The salting-out effect and phase separation in aqueous solutions of electrolytes and poly(ethylene glycol), *Polymer*, 2005, **46**(8), 2567–2572, DOI: 10.1016/j.polymer.2005.02.019.
67 Ł. Otulakowski, M. Kasprów, A. Strzelecka, A. Dworak and B. Trzebicka, Thermal behaviour of common thermoresponsive polymers in phosphate buffer and in its salt solutions, *Polymers*, 2020, **13**(1), 90.
68 Q. Li, L. Wang, F. Chen, A. P. Constantinou and T. K. Georgiou, Thermoresponsive oligo (ethylene glycol) methyl ether methacrylate based copolymers: Composition and comonomer effect, *Polym. Chem.*, 2022, **13**(17), 2506–2518.
69 R. Gómez-Bombarelli, E. Calle and J. Casado, Mechanisms of Lactone Hydrolysis in Neutral and Alkaline Conditions, *J. Org. Chem.*, 2013, **78**(14), 6868–6879, DOI: 10.1021/jo400258w.
70 C.-G. Zhan, D. W. Landry and R. L. Ornstein, Theoretical Studies of Fundamental Pathways for Alkaline Hydrolysis of Carboxylic Acid Esters in Gas Phase, *J. Am. Chem. Soc.*, 2000, **122**(7), 1522–1530, DOI: 10.1021/ja993311m.
71 C.-G. Zhan, D. W. Landry and R. L. Ornstein, Energy Barriers for Alkaline Hydrolysis of Carboxylic Acid Esters in Aqueous Solution by Reaction Field Calculations, *J. Phys. Chem. A*, 2000, **104**(32), 7672–7678, DOI: 10.1021/jp001459i.
72 Q. Zhu, F. Qiu, B. Zhu and X. Zhu, Hyperbranched polymers for bioimaging, *RSC Adv.*, 2013, **3**(7), 2071–2083, DOI: 10.1039/C2RA22210H.
73 S. Grimme, J. Antony, S. Ehrlich and H. Krieg, A consistent and accurate ab initio parametrization of density functional dispersion correction (DFT-D) for the 94 elements H-Pu, *J. Chem. Phys.*, 2010, **132**, 154104, DOI: 10.1063/1.3382344.
74 S. Grimme, S. Ehrlich and L. Goerigk, Effect of the damping function in dispersion corrected density functional theory, *J. Comput. Chem.*, 2011, **32**(7), 1456–1465, DOI: 10.1002/jcc.21759.
75 F. Weigend and R. Ahlrichs, Balanced basis sets of split valence, triple zeta valence and quadruple zeta valence quality for H to Rn: Design and assessment of accuracy, *Phys. Chem. Chem. Phys.*, 2005, **7**(18), 3297–3305, DOI: 10.1039/B508541A.

76 D. Rappoport and F. Furche, Property-optimized Gaussian basis sets for molecular response calculations, *J. Chem. Phys.*, 2010, **133**, 134105, DOI: 10.1063/1.3484283.
77 G. Scalmani and M. J. Frisch, Continuous surface charge polarizable continuum models of solvation. I, General formalism, *J. Chem. Phys.*, 2010, **132**, 114110, DOI: 10.1063/1.3359469.
78 M. Zeeshan and B. Gurkan, Sorbent Regeneration via Radiofrequency-Assisted Dielectric Heating for Direct Air Capture of CO2, *ACS Appl. Eng. Mater.*, 2025, **3**(4), 798–802, DOI: 10.1021/acsaenm.5c00202.
79 C. Gabriel, S. Gabriel, E. H. Grant, E. H. Grant, B. S. J. Halstead and D. M. P. Mingos, Dielectric parameters relevant to microwave dielectric heating, *Chem. Soc. Rev.*, 1998, **27**(3), 213–224, DOI: 10.1039/A827213Z.
80 T. Habib, N. Patil, X. Zhao, E. Prehn, M. Anas, J. L. Lutkenhaus, M. Radovic and M. J. Green, Heating of Ti3C2Tx MXene/polymer composites in response to Radio Frequency fields, *Sci. Rep.*, 2019, **9**(1), 16489, DOI: 10.1038/s41598-019-52972-2.
81 A. Jonderian and R. Maalouf, Formulation and In vitro Interaction of Rhodamine-B Loaded PLGA Nanoparticles with Cardiac Myocytes, *Front. Pharmacol.*, 2016, **7**, 458, DOI: 10.3389/fphar.2016.00458.
82 G. R. Bardajee, M. Bayat, S. Nasri and C. Vancaeyzeele, pH-Responsive fluorescent dye-labeled metal-chelating polymer with embedded cadmium telluride quantum dots for controlled drug release of doxorubicin, *React. Funct. Polym.*, 2018, **133**, 45–56, DOI: 10.1016/j.reactfunctpolym.2018.09.008.